Aeroacoustics Conferences
26-29 May 2026, Brussels, Belgium
32nd AIAA/CEAS Aeroacoustics Conference (2026)

10.2514/6.2026-3278

Large-eddy simulations of screeching jets impinging on a flat plate

Émilian De Staercke* and Christophe Bogey†
Ecole Centrale de Lyon, CNRS, Universite Claude Bernard Lyon 1, INSA Lyon, LMFA, UMR5509, 69130, Ecully, France

Large-eddy simulations are performed to investigate the properties of the screech and impingement tones produced by screeching jets impinging on a flat plate. The jets have a nozzle-exit Mach number $\mathrm{M}_e = 1$, a fully expanded Mach number equal to $\mathrm{M}_j = 1.13$ or 1.20 and a stagnation temperature equal to the ambient temperature. The nozzle-to-plate distance L varies between $5r_0$ and $16r_0$, where r_0 is the jet nozzle-exit radius. The corresponding free jets generate axisymmetric screech modes A1 and A2 for $\mathrm{M}_j = 1.13$ and 1.20, respectively. For the impinging jets, screech and impingement tones can both be found. The screech tones are dominant and coexist with impingement tones for nozzle-to-plate distances $L \gtrsim 10r_0$ for $\mathrm{M}_j = 1.13$ and $L \gtrsim 12r_0$ for $\mathrm{M}_j = 1.20$. For shorter distances, the impingement tones are stronger than the screech tones, whose amplitude becomes significantly weaker as the jet nozzle exit is closer to the plate. The impingement tones belong to the axisymmetric or the first helical mode. For a given Mach number, their frequencies exhibit a staging phenomena and their amplitudes fluctuate over a range of 30 dB as the nozzle-to-plate distance varies. The amplitudes are low when the nozzle-to-plate distance encompasses an integer number of the shock cells in the corresponding free jets, and high when it encompasses a half-integer number of cells. The stand-off shock near the plate is close to the last shock of the shock-cell network in the former case, whereas it is far in the latter. This suggests that the stand-off shock is involved in the near-plate generation mechanism of the upstream-propagating components of the feedback loops in impinging non-ideally expanded jets.

I. Introduction

Non-ideally expanded supersonic jets can be subject to an aeroacoustic resonance phenomenon causing the production of an intense tonal noise named screech. This phenomenon was first discovered by Powell [1, 2] and then studied by a large number of authors as highlighted in the reviews of Raman [3, 4] and more recently of Edgington-Mitchell [5]. They showed that in screeching jets an aeroacoustic feedback loop establishes between the nozzle and the shock cells in the jet potential core, and involves downstream-propagating Kelvin–Helmholtz instability waves and upstream-propagating acoustic waves. The screech resonance phenomenon is organized into modes, namely the axisymmetric modes A1 and A2, the flapping modes B and D, and the helical mode C, whose presence depends on the jet Mach number. They are characterized by a specific azimutal structure and feedback frequency. For each mode, the generated noise is radiated in far-field and has a specific directivity which differs between the fundamental and the harmonic tones [6, 7]. In the case of impinging jets, a strong tonal noise can also be generated [5], even if the jet is ideally expanded [8, 9] or subsonic [10]. This tonal noise is also produced by an aeroacoustic feedback loop similar to that of the screech, but establishing between the nozzle and the plate [9, 11].

Recently, for both screech [12, 13] and impingement resonance [9, 14], it was shown that the upstream component of the feedback loops consists of upstream-propagating guided jet waves. These waves are mainly confined inside the jet potential core, have a weak but non-negligible amplitude just outside, and only exist over narrow frequency bands [14, 15]. For screech resonance, the mechanism which produces the upstream-travelling component is known to be the interactions of instability waves with the first shock cells in the jet potential core [1, 2, 16], most probably occuring at the shock tips [3, 5]. For nozzle-to-plate resonance, multiple noise production mechanisms have been reported in the literature, including the impact of large-scale coherent structures on the plate [17], the oscillation of the wall-jet boundary [18], the wall-jet shocklet [19] and the leakage of the stand-off shock through the jet shear layer [20].

*PhD Student, emilian.de-staercke@ec-lyon.fr
†CNRS Research Scientist, christophe.bogey@ec-lyon.fr, AIAA Associate Fellow.

Several resonant modes can simultaneously exist for a given Mach number in screeching and impinging jets. They are due to different feedback loops establishing in the flow [5], each with its own azimutal structure, upstream- and downstream-propagating disturbances and downstream noise production mechanism [21]. In the case of underexpanded impinging jets, screech and nozzle-to-plate resonance can coexist in the flow [22, 23]. Triadic interactions can occur between screech and impingement modes [24, 25], and also between impingement modes [26], thus generating additional tones. In the case of rectangular underexpanded jets, Norum [27] observed that, for Mach numbers between $M_j = 0.98$ and 1.95 and nozzle-to-plate distances between $L = 4$ and 17 nozzle widths, the frequencies of the dominant impingement tones are close to the screech frequency of the corresponding free jet, when a screech tone is present. In the case of round ideally expanded jets with a Mach number $M_j = 1.5$, Krothapalli et al. [28] found that the impingement tone frequencies are scattered around the screech frequency of the corresponding underexpanded jet. For round underexpanded jets with Mach numbers between $M_j = 1.36$ and 1.56 and nozzle-to-plate distances between $L = 3r_0$ and $10r_0$, Henderson et al. [18] reported the absence of tones over wide ranges of nozzle-to-plate distances depending on the Mach number, for $5.4 \lesssim L/r_0 \lesssim 7$ at $M_j = 1.56$ for example, and noted that there is no tone when the plate is located in a compression region of the shock-cell network of the corresponding free jet. Numerous authors then studied the configurations of Henderson et al. [18] using large-eddy simulations. Dauptain et al. [29] obtained, for $M_j = 1.56$, tones for $L = 4.16r_0$ but not for $L = 8.32r_0$. For the same Mach number, Gojon and Bogey [30] found tones for $L = 4.16r_0$, $5.6r_0$ and $9.32r_0$ but not for $L = 8.32r_0$, in agreement with Henderson et al. [18]. More recently, Jia and Gao [31] reported, for a nozzle-to-plate distance $L = 4.16r_0$ and for Mach numbers between $M_j = 1.19$ and 1.76, no tones for $1.38 \lesssim M_j \lesssim 1.49$, but tones are present for $M_j = 1.56$, in agreement with Henderson et al. [18]. Finally, in their experimental study, Mancinelli et al. [25] observed a "competition phenomenon" between screech and impingement resonances as the nozzle-to-plate distance varies between $L = 6r_0$ and $20r_0$, for Mach numbers between $M_j = 1$ and 1.5. More precisely, when the plate is very close to the nozzle, for $L \lesssim 4r_0$, no screech tone can be found. However, as the nozzle-to-plate distance increases, screech tones appears. For example, screech tones belonging to mode A1 are observed for $L \simeq 8r_0$ at $M_j \simeq 1.1$. When the nozzle-to-plate distance is sufficiently large, for $L \gtrsim 20r_0$, impingement tones do not appear and only screech tones emerge.

In the present work, underexpanded supersonic jets impinging on a flat plate are computed using large-eddy simulations (LES) to investigate the properties of screech and impingement tones in such jets. More precisely, the aim is to study the coexistence and the properties of the screech and impingement tones as the nozzle-to-plate distance varies. Another objective is to characterize and explain the presence or absence of tones that may be observed for certain ranges of nozzle-to-plate distance. The jets have a nozzle-exit Mach number of $M_e = 1$ and ideally expanded Mach numbers equal to $M_j = 1.13$ and 1.20, yielding underexpanded supersonic jets generating screech modes A1 and A2. Their stagnation temperature is equal to the ambient temperature, leading to cold jets, and their diameter-based Reynolds number is close to $\mathrm{Re}_D \simeq 4 \times 10^5$. The nozzle-to-plate distance varies between $L = 5r_0$ and $16r_0$. Thus, the jets are similar to those studied experimentally by Mancinelli et al. [25], and they have smaller Mach numbers than those in Henderson et al. [18]. To identify the effects of the plate on screech noise, free jets are also simulated for the two Mach numbers. The main flow features are examined using snapshots of vorticity and pressure fluctuations. Acoustic spectra with azimutal mode decompositions are computed in the near-nozzle region to characterize the tones. The variations of the tone frequencies with the nozzle-to-plate distance are described and compared with the screech frequencies in the free jets and with the predictions provided by an aeroacoustic feedback loop model in an impinging jet to discuss the nature of each tone. The variations of the amplitudes of the dominant tones as a function of the nozzle-to-plate distance are then addressed. Mean pseudo-schlieren fields are provided to visualize the shocks, and determine their positions. Finally, links between the ranges of nozzle-to-plate distances where the tones can or cannot be observed and the positions of the plate and the shocks are sought.

This paper is organized as follows. In section II, the jet initial conditions are defined, and the large-eddy simulation methods and parameters are documented. Results are presented in section III,.

II. Methods and parameters

A. Jet parameters

The jets have ideally expanded Mach numbers $M_j = u_j/c_j$ equal to 1.13 and 1.20, a temperature $T_j = T_0/(1 + M_j^2(\gamma-1)/2)$ and a Reynolds number $\mathrm{Re}_D = u_j D/\nu_j \simeq 4\times10^5$, where u_j, c_j and ν_j are the ideally expanded jet velocity, the sound speed and the kinematic viscosity, D is the nozzle diameter, $\gamma = 1.4$ is the isentropic coefficient and T_0 is the ambient temperature. The Mach numbers were chosen to consider jets generating screech tones of modes A1 and A2. The flow originates at $z = 0$ with a Mach number of 1 from a straight pipe nozzle of radius $r_0 = D/2 = 6$ mm and length $10r_0$, whose lip is $0.15r_0$ thick, into an ambient medium at rest at pressure $p_0 = 10^5$ Pa and temperature $T_0 = 295$ K. Thus, the jets are cold, underexpanded at the nozzle exit and have a total temperature equal to the ambient temperature. The flow impinges on a flat plate perpendicular to the jet axis located at a distance $z = L$ from the nozzle varying between $5r_0$ and $16r_0$. The jet Mach numbers and the nozzle-to-plate distances used for each LES are represented in figure 1. The nozzle-to-plate distance ranges from $L = 5r_0$ to $16r_0$ for $\mathrm{M}_j = 1.13$ and from $L = 7r_0$ to $14r_0$ for $\mathrm{M}_j = 1.20$.

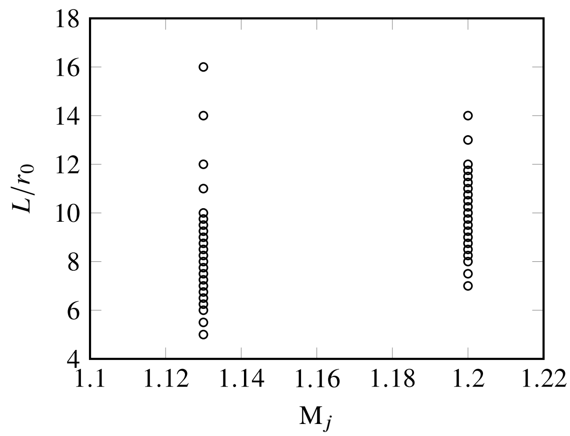

Fig. 1 Jet Mach numbers M_j and nozzle-to-plate distances L.

In the pipe, at $z = -2r_0$, a Blasius laminar boundary-layer profile of thickness $\delta_{\mathrm{BL}} = 0.1r_0$ is imposed for the axial velocity, radial and azimuthal velocities are set to zero, pressure is equal to $p_0(1 + \mathrm{M}_j^2(\gamma - 1)/2)/(1 + (\gamma - 1)/2)$ and temperature is equal to $T_0/(1 + (\gamma - 1)/2)$ outside the boundary layer. The temperature within the boundary layer is determined using a Crocco–Busemann relation. The boundary layers are tripped at $z = -0.5r_0$ leading to weakly disturbed flow conditions at the exit with a peak turbulent fluctuations intensity close to $\langle u_z' u_z' \rangle^{1/2}/u_j = 3$ %, where u_z' is the axial turbulent velocity fluctuation and $\langle . \rangle$ is the time averaging operator. To illustrate the nozzle-exit conditions, the radial profiles of mean and root-mean-squared values of axial velocity obtained at the nozzle-exit for Mach numbers $\mathrm{M}_j = 1.13$ and 1.20 and for nozzle-to-plate distances $L = 8r_0$, $10r_0$ and $12r_0$ are represented in figure 2. In figure 2(a), the profiles of mean axial velocity have a similar shape. They differ from the Blasius profile imposed inside the pipe due to the expansion occurring at the nozzle exit since the jet is underexpanded. In figure 2(b), the profiles of root-mean-squared axial velocity are nearly superimposed. The turbulent intensities are significant in the boundary layer and reach a peak value equal to 3 % of u_j, as expected.

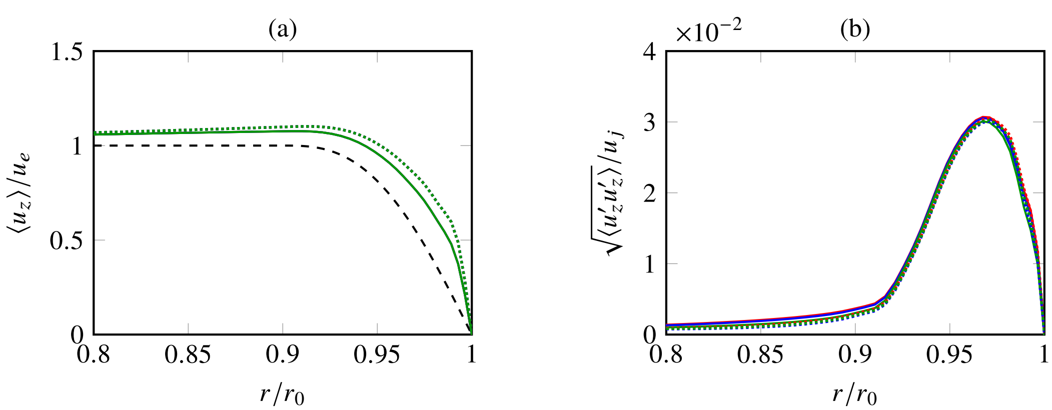

Fig. 2 Radial profiles of (a) mean and (b) rms axial velocity at $z = 0$ for the impinging jets for (solid lines) M_j = 1.13 and (dotted lines) M_j = 1.20 for (red) $L = 8r_0$, (blue) $L = 10r_0$ and (green) $L = 12r_0$; - - - - Blasius laminar boundary layer for $\delta_{\mathrm{BL}} = 0.1r_0$.

B. Numerical methods and parameters

The large-eddy simulations have been carried out by solving the three-dimensional filtered compressible Navier–Stokes equations in cylindrical coordinates (r, θ, z) based on low-dissipation and low-dispersion explicit schemes [9, 32]. Spatial derivatives are computed using a fourth-order eleven-point centered finite difference scheme, time integration is performed using a second-order six-stage Runge–Kutta algorithm and grid-to-grid oscillations are removed using a sixth-order eleven-point centered filter [33]. The filtering is used as a subgrid-scale high-order dissipation model relaxing turbulent energy at wavenumbers close to the grid cutoff wavenumber while leaving larger scales mostly unaffected [34]. Non-centered finite difference schemes and filters are employed near walls and grid boundaries [35]. To remove Gibbs oscillations around the shocks, a shock-capturing method based on a conservative adaptative second-order filtering is employed [36]. Near the axis, the singularity is taken into account by using the method of Mohseni and Colonius [37] and the time-step restriction is reducing by computing the azimuthal derivatives at a coarser resolution [38]. At the grid boundaries, radiation conditions [39] are applied along with sponge zones combining grid stretching and Laplacian filtering. In the pipe, the tripping of the boundary layers is performed by adding random low-level vortical disturbances uncorrelated in the azimuthal direction [32]. No co-flow is imposed.

The meshes are similar to those used in previous work on free [13, 40] and impinging [17, 20] jets. In the radial direction, the meshes are identical and extend up to $r = 15r_0$, excluding the sponge zone spreading up to $20r_0$ for the free jets and up to $30r_0$ for the impinging jets, and contain $n_r = 528$ and 587 points, respectively. The radial mesh spacing is minimal and equal to $\Delta r = 0.0036r_0$ at $r = r_0$, and is equal to $\Delta r = 0.075r_0$ between $r = 6.4r_0$ and $15r_0$, allowing to propagate acoustic waves up to a Strouhal number $\mathrm{St}_D = fD/u_j = 5$, where f is the frequency, using 5 points per wavelength. In the azimutal direction, the mesh spacing is constant and $n_\theta = 512$ points are used. In the axial direction, the meshes extend from $z = -10r_0$ to $z = L$ in the impinging cases and to $z = 50r_0$ in the free cases, excluding the sponge layers spreading down to $z = -20r_0$ for all cases and up to $z = 120r_0$ for the free case. The number of points varies between $n_z = 893$ for $L = 5r_0$ and $n_z = 1682$ for $L = 16r_0$ in the impinging cases, and is equal to $n_z = 2571$ in the free cases. Overall, the meshes contain between 268 and 695 million points.

The simulations were performed using an in-house MPI-CUDA solver running on multiple GPU nodes. They are first run for a time $T = 400r_0/u_j$ to evacuate the transient regime, and then for a time $T = 2000r_0/u_j$ to obtain converged accoustic spectra. The computational cost is around 600 GPU hours for a free jet and around 250 GPU hours for an impinging jet with $L = 5r_0$.

III. Results

First, to describe the screech tones occurring without flat plate, the acoustic spectra obtained in the near-nozzle region of the free jets at Mach numbers $\mathrm{M}_j = 1.13$, 1.15 and 1.20 are represented in figure 3. The spectra are calculated for the full pressure signals and their decomposition along the first three azimutal modes. For $\mathrm{M}_j = 1.13$ and 1.20, in figures 3(a,c), an axisymmetric screech tone is dominant in the spectra. It emerges above the broadband noise by more than 35 dB at a Strouhal number $\mathrm{St}_D \simeq 0.639$ for $\mathrm{M}_j = 1.13$ and at $\mathrm{St}_D \simeq 0.589$ for $\mathrm{M}_j = 1.20$. Its first harmonic is also observed, at $\mathrm{St}_D \simeq 1.218$ and 1.178, respectively. The tone is emitted by a screech modes A1 in the first case and a screech mode A2 in the second case. For $\mathrm{M}_j = 1.15$, in figure 3(b), screech tones A1 and A2 both exist. They emerge at $\mathrm{St}_D \simeq 0.618$ and 0.679 by approximately 20 dB, respectively. This is expected due to the staging phenomenon occuring between the two modes when the Mach number varies between $\mathrm{M}_j = 1.13$ and 1.20 [4, 5]. In addition to the screech tones, weaker peaks appear for the three Mach numbers. They either belong to the axisymmetric mode, at $\mathrm{St}_D \simeq 0.274$ and 1.14 for $\mathrm{M}_j = 1.13$ and at $\mathrm{St}_D \simeq 0.250$ and 0.981 for $\mathrm{M}_j = 1.20$ for instance, or to the first helical mode, at $\mathrm{St}_D \simeq 0.476$ and 0.807 for $\mathrm{M}_j = 1.13$ and at $\mathrm{St}_D \simeq 0.435$ and 0.981 for $\mathrm{M}_j = 1.20$ for example. These peaks may be the signature of the freestream upstream-propagating guided jet waves [41] or may be due to secondary screech resonances.

To illustrate the main flow features of the impinging jets, snapshots of vorticity and pressure fluctuations in the (r, z) plane are provided in figure 4 for the nozzle-to-plate distances $L = 8r_0$, $9r_0$ and $10r_0$ and for the jet Mach numbers $\mathrm{M}_j = 1.13$ and 1.20. In all cases, the mixing layers thicken downstream of the nozzle and transition to turbulence. They impinge on the flat plate, before the closing of the potential core, and then generate a wall-jet which spreads radially over the plate. Strong pressure fluctuations are observed in all cases, especially in the jet potential core. Large-scale coherent structures develop in the mixing layers and in the wall-jet as a succession of under- and over-pressure spots. Outside the jet, high-frequency noise is observed. More strikingly, near the jet, upstream-propagating wavefronts with a characteristic wavelength in all cases are clearly observed, indicating that tonal noise is produced. For $\mathrm{M}_j = 1.13$, in figures 4(a–c), the wavefronts are symmetrical with respect to the jet axis. For $\mathrm{M}_j = 1.20$, in figure 4(d–f), the fronts

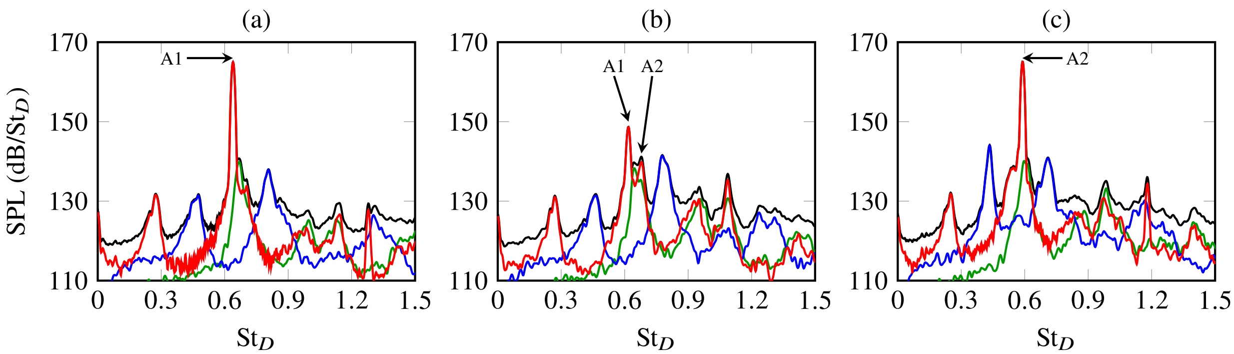

Fig. 3 Acoustic spectra obtained at $r = 1.5r_0$ and $z = 0$ for the free jets with (a) $M_j = 1.13$, (b) $M_j = 1.15$ and (c) $M_j = 1.20$: —— full spectra, —— $n_\theta = 0$, —— $n_\theta = 1$ and —— $n_\theta = 2$.

are symmetrical for $L = 8r_0$ and $12r_0$ and antisymmetrical for $L = 10r_0$. The degree of emergence of the wavefronts also greatly varies. Tey are very strong for $M_j = 1.20$ and $L = 10r_0$ in figure 4(e), moderate for $M_j = 1.13$ in figures 4(a–c) and weak for $M_j = 1.20$ and $L = 12r_0$ in figure 4(f).

In order to characterize the shock-cell network, the mean pressure profiles obtained along the jet axis for the impinging jets for nozzle-to-plate distances from $L = 8r_0$ to $12r_0$ with an increment $\Delta L = r_0$ are represented in figure 5(a) for $M_j = 1.13$ and in figure 5(b) for $M_j = 1.20$. The mean pressure profiles obtained for the corresponding free jets are also represented. In all cases, the mean pressure is constant and higher than the ambient pressure in the nozzle, for $z \lesssim 0$, because the jets are underexpanded. Downstream of the nozzle-exit, for $z \gtrsim 0$, the mean pressure oscillates around the ambient pressure, yielding a succession of compression and expansion regions which forms the shock-cell network. For the free jets, the amplitudes of the oscillations decrease with the axial position. For the impinging jets, the mean pressure varies as for the free jets far from the plate. Near the plate, the mean pressure increases between $z \simeq L - 1.5r_0$ and L up to the jet stagnation pressure. It can be noted that, for the impinging jet with $L = 9r_0$ and $M_j = 1.20$, the mean pressure profile differs significantly than that for the free jets between $z \simeq 3r_0$ and $8r_0$. As it will be shown in figure 7(e), this is due to the presence of a very intense tone for $n_\theta = 1$ yielding strong large coherent structures at the tone frequency in the mixing layers, whose convection makes the shock-cell network oscillate.

The lengths of the shock cells obtained for the free jets considered in figure 5 are represented in figure 6. The shock cells are numbered in ascending order with increasing axial position. The shock-cell lengths predicted using the model of Harper-Bourne and Fisher [42]

$$L_s = 1.1D\sqrt{M_j^2 - 1} \tag{1}$$

are also indicated. The lengths of the shock cells vary between $L_s \simeq r_0$ and $1.3r_0$ for $M_j = 1.13$ and between $L_s \simeq 1.1r_0$ and $1.6r_0$ for $M_j = 1.20$. They are similar to the lengths predicted by the model. For the free jets, for $M_j = 1.13$, the shock-cell lengths increase from the first to the third cell and then decrease. For $M_j = 1.20$, they increase from the first to the second cell and then decrease. For the impinging jets, they are similar to those for the free jets, especially for the cells that are far from the plate. For $M_j = 1.20$ and $L = 9r_0$, in particular, the shock-cell lengths differ significantly from the those for the other jets.

Regarding the noise generated by the impinging jets, the acoustic spectra computed in the near-nozzle region for Mach numbers $M_j = 1.13$ and 1.20 and for nozzle-to-plate distances $L = 8r_0$, $9r_0$ and $10r_0$ are represented in figure 7 along with the contributions of the first three azimutal modes. The spectra obtained for the corresponding free jets are also shown. Several tones are found for all impinging jets for modes $n_\theta = 0$ and 1. For $M_j = 1.13$, in figures 7(a–c), the dominant tones are obtained for the axisymmetric mode. For $L = 10r_0$, in figure 7(c), its frequency and amplitude are similar to those of the screech tone A1 obtained for the free jet, suggesting that it is of the same nature. For $L = 8r_0$ and $9r_0$, in figures 7(a,b), the dominant tones have a lower frequency and a slightly higher amplitude than those of the screech tone A1 of the free jet, suggesting that it is produced by a feedback machanism different from that occuring for $L = 10r_0$. For $M_j = 1.20$, in figures 7(d–f), the dominant tones seem more sensitive to the nozzle-to-plate distance than for $M_j = 1.13$. For $L = 8r_0$, in figure 7(d), the dominant tone is axisymmetric and is found at a frequency very close to that of the screech mode A2 of the free jet, but its amplitude is slightly higher. For $L = 9r_0$, in figure 7(e), the dominant tone is helical and emerges by more than 35 dB from the broadband noise at $St_D \simeq 0.435$. A strong

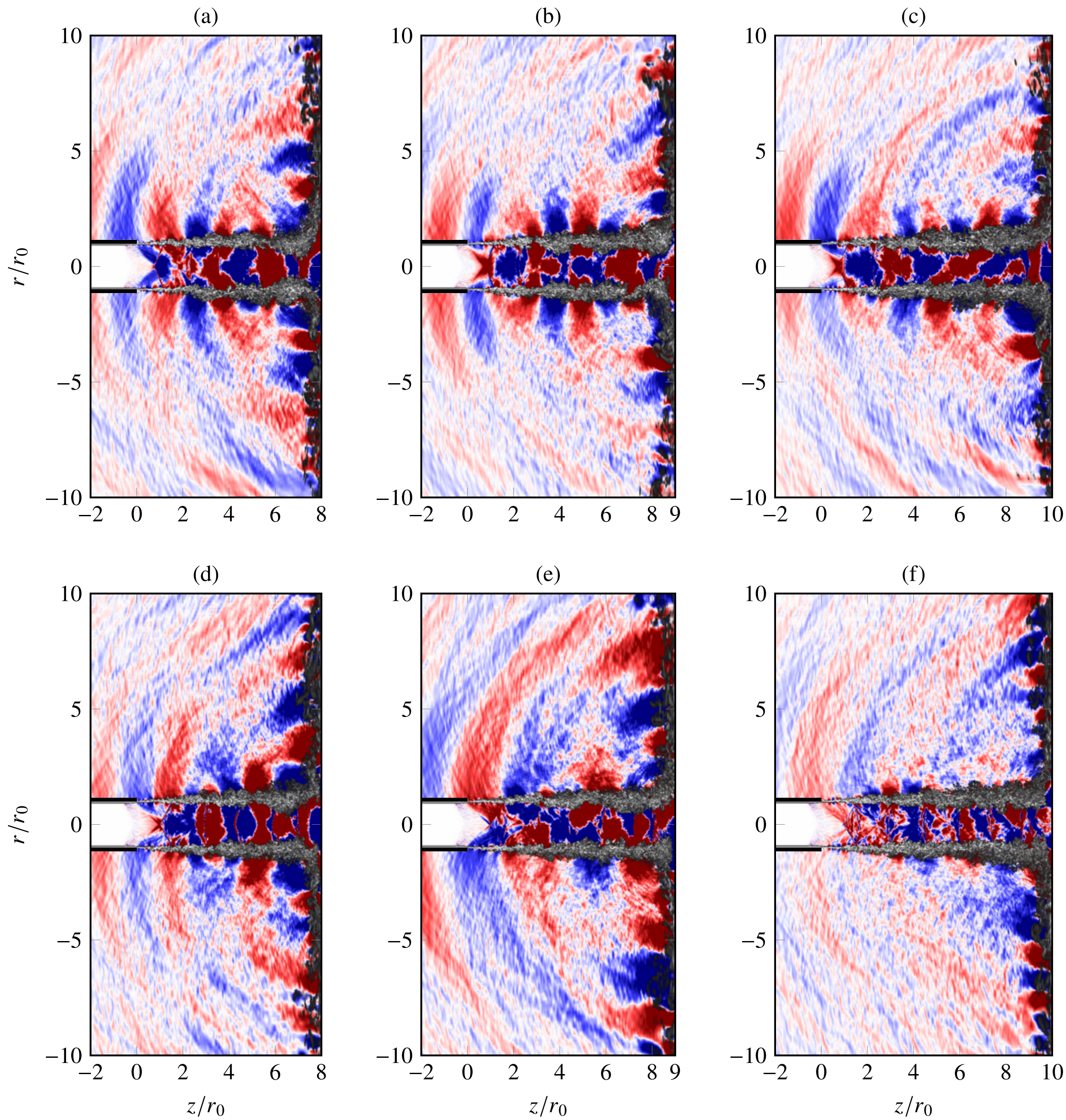

Fig. 4 Snapshots of pressure fluctuations and vorticity in the (r, z) plane for the impinging jets for (a–c) $\mathrm{M}_j = 1.13$ and (d–f) $\mathrm{M}_j = 1.20$ and for (a,d) $L = 8r_0$, (b,e) $L = 9r_0$ and (c,f) $L = 10r_0$; the color scale spans from blue to red over ±2000 Pa for pressure and from black to white, from 0 to $20u_j/r_0$, for vorticity.

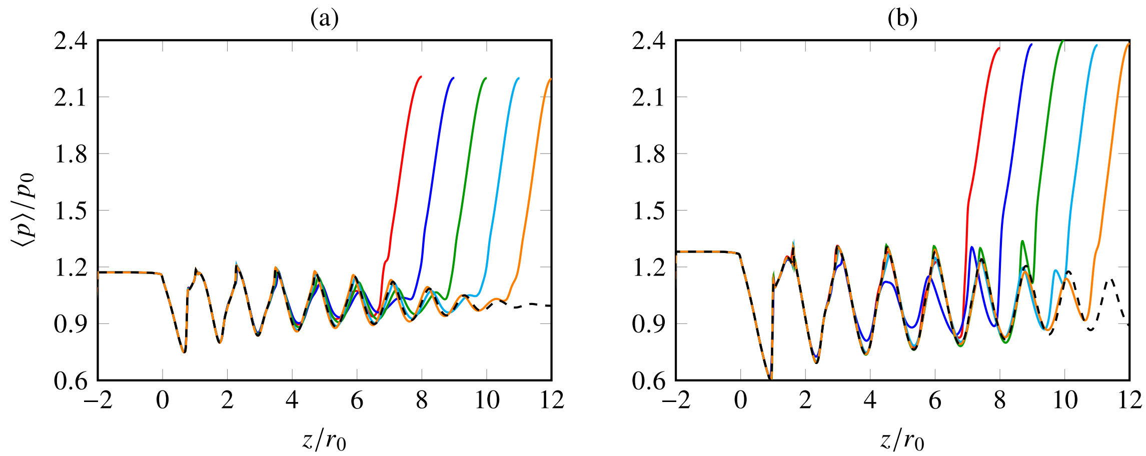

Fig. 5 Mean pressure profiles along the jet axis for (a) $M_j = 1.13$ and (b) $M_j = 1.20$ for - - - - free jets, impinging jets for —— $L = 8r_0$, —— $L = 9r_0$, —— $L = 10r_0$, —— $L = 11r_0$ and —— $L = 12r_0$.

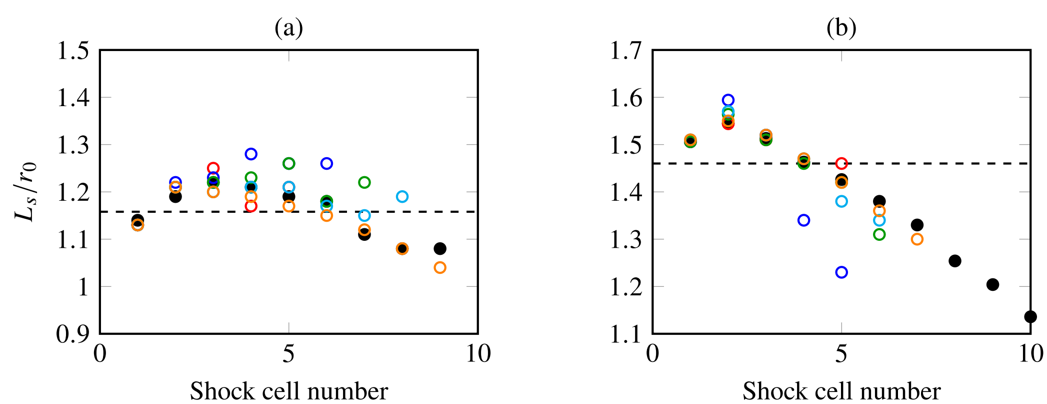

Fig. 6 Shock-cell lengths for (a) $M_j = 1.13$ and (b) $M_j = 1.20$ for ● free jets, impinging jets for ○ $L = 8r_0$, ○ $L = 9r_0$, ○ $L = 10r_0$, ○ $L = 11r_0$ and ○ $L = 12r_0$; - - - - length predicted from Eq. (1).

first harmonic belonging to the second helical mode is also observed. No tone with a frequency close to that of the screech tone A2 of the free jet can be found. For $L = 10r_0$, in figure 7(f), the tones are at least 20 dB lower in amplitude compared to the tones in the two previsou figures. Again, no tone with a frequency close to that of the screech tone A2 appears.

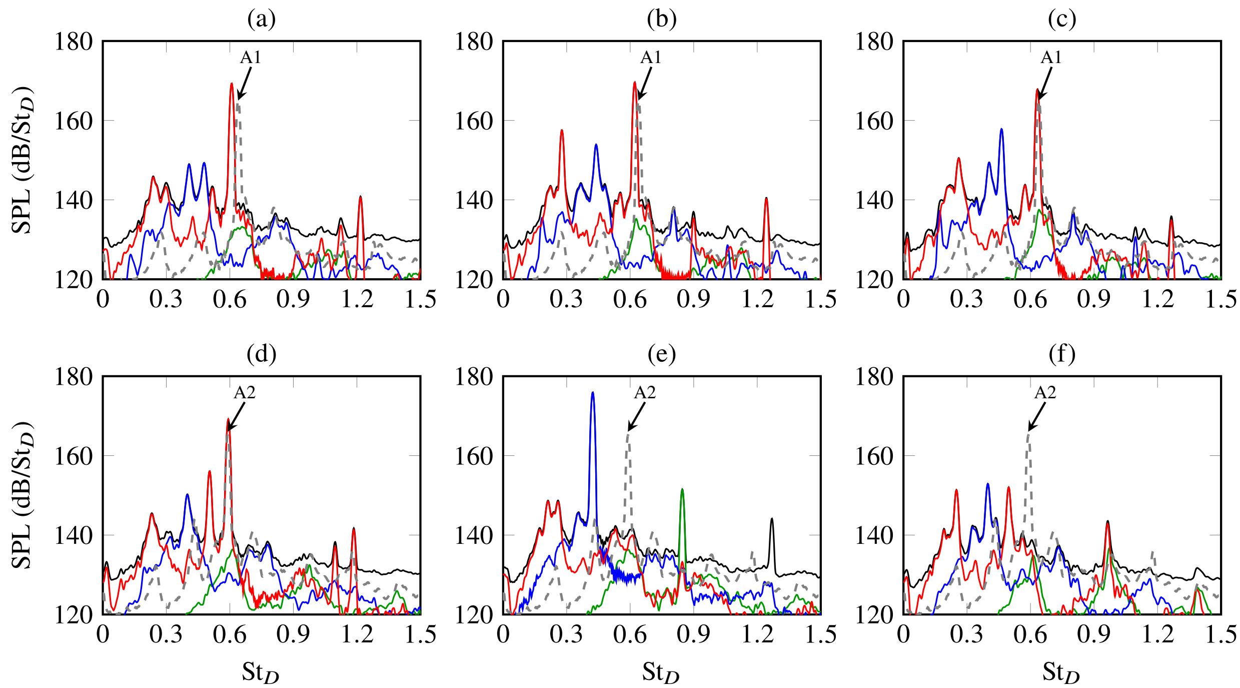

Fig. 7 Acoustic spectra obtained at $r = 1.5r_0$ and $z = 0$ for the impinging jets at (a–c) $\mathrm{M}_j = 1.13$ and (d–f) $\mathrm{M}_j = 1.20$ for (a,d) $L = 8r_0$, (b,e) $L = 9r_0$ and (c,f) $L = 10r_0$: —— total, —— $n_\theta = 0$, —— $n_\theta = 1$ and —— $n_\theta = 2$; - - - - full spectra for the corresponding free jets.

The frequencies of the tones for $n_\theta = 0$ and 1 are represented as a function of the nozzle-to-plate distance in figure 8(a) for $\mathrm{M}_j = 1.13$ and in figure 8(b) for $\mathrm{M}_j = 1.20$. They are compared with the screech frequencies for the corresponding free jets, equal to $\mathrm{St}_D = 0.639$ for $\mathrm{M}_j = 1.13$ and to $\mathrm{St}_D = 0.589$ for $\mathrm{M}_j = 1.20$. They are also compared with the predictions given by the feedback loop model

$$\mathrm{St}_D = \frac{n u_c D}{L u_j (u_c/c_{\mathrm{amb}} + 1)} \tag{2}$$

for the nozzle-to-plate resonance, assuming downstream-propagating Kelvin–Helmholtz instability waves with a convection velocity $u_c = 0.7u_j$ and acoustic waves propagating upstream at the ambient speed of sound c_{amb} between the nozzle and the plate, n being the mode number. For the two Mach numbers, the frequencies of most of the tones are in agreement or very close to the predictions provided by Eq. (2), indicating that these tones result from nozzle-to-plate resonances. A few exceptions are for the dominant axisymmetric tones at $\mathrm{St}_D = 0.64$ for $L \gtrsim 11r_0$, in figure 8(a), and at $\mathrm{St}_D = 0.59$ for $L \gtrsim 13r_0$, in figure 8(b). Their frequencies are in agreement with the free-jet screech frequencies, suggesting that they are screech tones. Hence, the "competition phenomenon" between screech and impingement tones reported by Mancinelli et al. [25] is also found in the present simulations. For the two Mach numbers, the dominant tone exhibits a staging phenomenon when the nozzle-to-plate distance increases. For $\mathrm{M}_j = 1.13$, in figure 8(a), the dominant tone for $L \lesssim 10r_0$ is axisymmetric and close to the free-jet screech frequency except when staging occurs. The staging happens for $L = 7r_0$, $8.25r_0$ and $9.5r_0$ from modes $n = 5$ to 6, $n = 6$ to 7 and $n = 7$ to 8, respectively. In particular, for $L = 7r_0$ and $8.25r_0$, the dominant tone is associated with the first helical mode. Hence, the staging occurs for nozzle-to-plate distances separated by a length $\Delta L \simeq 1.25r_0$, which is close to the shock-cell length reported in figure 6(a). For $\mathrm{M}_j = 1.20$, in figure 8(b), the dominant tone exhibits a staging phenomenon between axisymmetric and first helical modes for $L \lesssim 12r_0$. Jumps from a first helical to an axisymmetric mode as the nozzle-to-plate distance increases occur at $L \simeq 8r_0$, $9.5r_0$ and $11.25r_0$. These nozzle-to-plate distances are separated by a length $\Delta L \simeq 1.5r_0$, which is also close to the shock-cell length reported in figure 6(b).

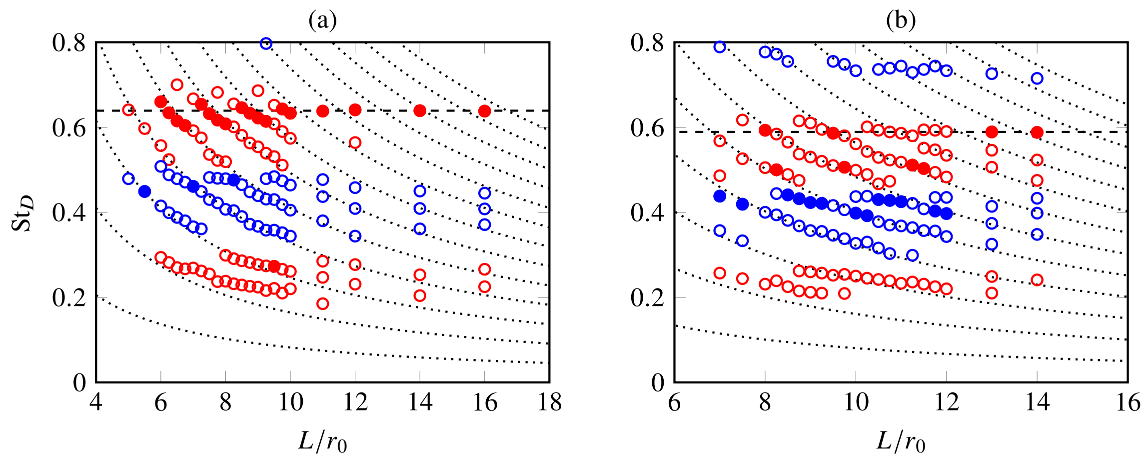

Fig. 8 Tone frequencies obtained at $r = 1.5r_0$ and $z = 0$ for (a) $M_j = 1.13$ and (b) $M_j = 1.20$ for (red) $n_\theta = 0$ and (blue) $n_\theta = 1$ as a function of the nozzle-to-plate distance L ; the marker is filled when the tone is dominant ; ········ predictions from Eq. (2) ; - - - - screech frequency for the free jets.

The amplitudes of the dominant tones for $M_j = 1.13$ and 1.20 are represented as a function of the nozzle-to-plate distance in figure 9. The nature of the tones, the axial positions of the shocks and the amplitude of the screech tones in the free jets are also indicated. For the two Mach numbers, the amplitude of the dominant tone fluctuates strongly with the nozzle-to-plate distance. When the dominant tone is an impingement tone, for $L \lesssim 10r_0$ in figure 9(a) and for $L \lesssim 12r_0$ in figure 9(b), its amplitude oscillates roughly between 150 and 175 dB. It reaches a minimum when the plate is close to a position of a shock in the free jet, i.e. when it is located in a compression region in the potential core. On the contrary, the dominant tone amplitude reaches a maximum when the plate is located between two consecutive free-jet shocks, i.e. when it is located in an expansion region. These two behaviors are in agreement with those reported by Henderson et al. [18] for an underexpanded supersonic jet at the Mach number $M_j = 1.56$ and for the nozzle-to-plate distances between $L = 3r_0$ and $10r_0$. When the dominant tone is a screech tone, for $L \gtrsim 10r_0$ at $M_j = 1.13$ and for $L \gtrsim 12r_0$ at $M_j = 1.20$, its amplitude does not vary much and converges to the amplitude of the free-jet screech tone as the nozzle-to-plate distance increases. For $M_j = 1.13$, the dominant tones are axisymmetric in most cases, but they can be associated with the first helical mode when their amplitudes are low. For $M_j = 1.20$, the dominant tones are most associated with the first helical mode, but they can be axisymmetric when their amplitudes decrease with the nozzle-to-plate distance.

Mean pseudo-schlieren fields calculated in the (r, z) plane for the impinging jets at $M_j = 1.13$ are represented in figure 10 for $L = 6r_0$, $6.25r_0$, $6.5r_0$, $6.75r_0$, $7r_0$, $7.25r_0$, $7.75r_0$ and $8.25r_0$. They correspond to the norm of the gradient in the (r, z) plane of the mean density. The axial positions of the last shocks of the shock-cell networks and of the stand-off shocks are indicated. The axial positions of the shock tips of the corresponding free jets are also represented. In all cases, a succession of shock cells is observed between the nozzle and the plate in the jet potential core. No Mach disk is observed, due to the low Mach numbers considered. Far from the plate, the axial positions of the shocks coincide with those for the free jets. Near the plate, the mixing layers are deviated away from the jet axis as the jets impinge on the plate. A stand-off shock is also present in front of the plate. Between $L = 6r_0$ and $7.25r_0$, in the first six figures, the amplitude of the dominant tone describes an oscillation period as reported in figure 9(a). For $L = 6r_0$, in figure 10(a), when the amplitude of the tone is low, the plate is near the fifth shock in the free jets, and the stand-off shock is close to the last shock of the impinging jet, which is the fourth shock. For $L = 6.25r_0$, $6.5r_0$ and $6.75r_0$ in figures 10(b–d), when the amplitude of the dominant tone is approximately 25 dB higher compared to $L = 6r_0$, the plate is located downstream of the fifth shock in the free jets, and the distance between the stand-off shock and the last shock increases with the nozzle-to-plate distance. For $L = 7r_0$ in figure 10(e), when the amplitude of the tone is low again, a fifth shock appears in the impinging jet. The distance between the last shock, which is now the fifth shock, and the stand-off shock is then much lower compared to $L = 6.75r_0$. For $L = 7.25r_0$ in figure 10(f), when the amplitude of the tone is still low, the plate is located slightly downstream of the sixth free-jet shock and the distance between the last shock and the stand-off

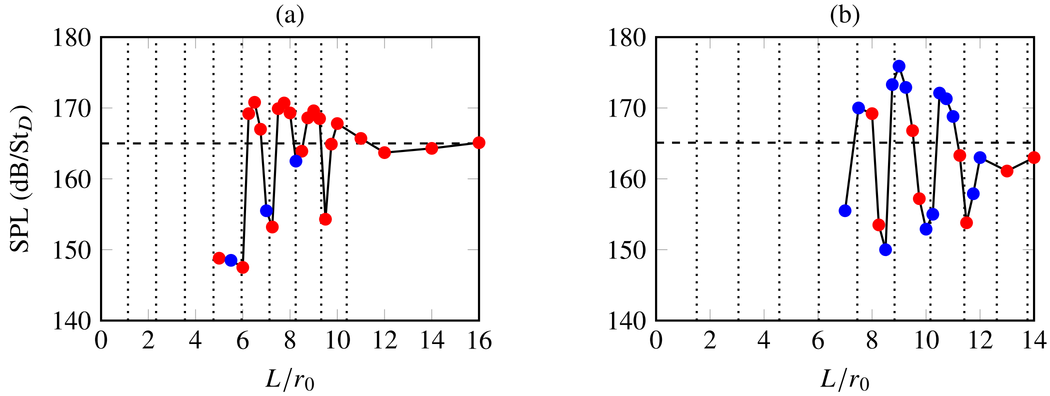

Fig. 9 Dominant tone amplitudes obtained at $r = 1.5r_0$ and $z = 0$ at (a) $M_j = 1.13$ and (b) $M_j = 1.20$ for ● $n_\theta = 0$ and ● $n_\theta = 1$ as a function of the nozzle-to-plate distance L ; ········ axial positions of the shocks for the corresponding free jets ; - - - - amplitudes of the free-jet screech tones.

shock is slightly higher compared to $L = 7r_0$. For $L = 7.75r_0$ and $8.25r_0$, in the two last figures, the amplitude of the tone reaches respectively a maximum and a minimum value as reported in figure 9(a). The distance between the last shock and the stand-off shock is higher for $L = 7.75r_0$ than for $L = 8.25r_0$. Furthermore, the plate is located between the sixth and the seventh shocks in the free jets for $L = 7.75r_0$, and near the seventh shock for $L = 8.25r_0$. These results show that, when the amplitude of the tone is high, the plate is located between two successive shocks in the free jets and the stand-off shock is far from the last shock in the impinging jets. On the contrary, when the amplitude of the tone is low, the plate is close to a shock in the free jets and the stand-off shock is close to the last shock in the impinging jets.

Mean pseudo-schlieren fields calculated in the (r, z) plane for the impinging jets at $M_j = 1.20$ are represented in figure 11 for $L = 7r_0$, $7.5r_0$, $8r_0$, $8.25r_0$, $8.5r_0$, $9r_0$, $9.5r_0$ and $10r_0$. The axial positions of the last shocks of the shock-cell network, of the stand-off shocks and of the free-jet shocks are also indicated. In all cases, a shock-cell network is present in the jet potential core and a stand-off shock is observed in front of the plate, as for $M_j = 1.13$ in figure 10. Between $L = 7r_0$ to $8.5r_0$, in figures 11(a–e), the amplitude of the tone describes an oscillation period, as reported in figure 9(b). Between $L = 8.5r_0$ to $10r_0$, in figures 11(e–h), it completes a second oscillation period. When the amplitude of the tone is low, for $L = 7r_0$, $8.25r_0$, $8.5r_0$ and $10r_0$, in figures 11(a,d,e,h), the distance between the last shock of the shock-cell network and the stand-off shock is small, and the plate is close to the position of a shock in the free jets. On the contrary, when the amplitude of the tone is high, for $L = 7.5r_0$, $8r_0$, $9r_0$ and $9.5r_0$, in figures 11(b,c,f,g), the distance between the last shock and the stand-off shock is large, and the plate is located between two consecutive shocks in the free jets. These trends are the same as those noted for $M_j = 1.13$ in figure 10.

The mean axial positions of the last shock in the shock-cell network for the impinging jets at $M_j = 1.13$ and 1.20 are represented as a function of the nozzle-to-plate distance in figure 12. The axial positions of the shocks in the free jets are also indicated. For the two Mach numbers, the axial position of the last shock increases with the nozzle-to-plate distance, but is always very close to the position of a shock in the free jets. As the nozzle-to-plate distance increases, the position of the last shock jumps from the position of a free-jet shock to the position of the next one in the network when the plate crosses a free-jet shock for $M_j = 1.13$ in figure 12(a), and when it reaches the middle between two consecutive free-jet shocks for $M_j = 1.20$ in figure 12(b).

The distances between the stand-off shock and the plate obtained for the impinging jets at $M_j = 1.13$ and 1.20 are represented as a function of the nozzle-to-plate distance in figure 13. The distances are normalized by the lengh of the local free-jet shock cell near the plate. The positions of the shocks in the free jets are also indicated. The normalized distances between the stand-off shock and the plate vary between 0.8 and 1.2 for $M_j = 1.13$ in figure 13(a), and between 0.6 and 1 for $M_j = 1.20$ in figure 13(b). For $M_j = 1.13$, they exhibit sharp peaks when the plate is close to the position of a free-jet shock, for instance for $L = 8r_0$ and $9.25r_0$. For $M_j = 1.20$, between $L = 6r_0$ and $10r_0$, the distances fluctuate in a saw-tooth manner, increasing smoothly with the nozzle-to-plate distance when the plate is located between two free-jet shocks but decreasing sharply when it crosses the position of a shock. This is in agreement with the observations of Henderson et al. [18], who also reported, for the impinging jets at $M_j = 1.56$, a jump of the stand-off shock close to the plate when the plate reaches a free-jet shock as the nozzle-to-plate distance increases.

The distances calculated between the last shock of the shock-cell network and the stand-off shock for the impinging

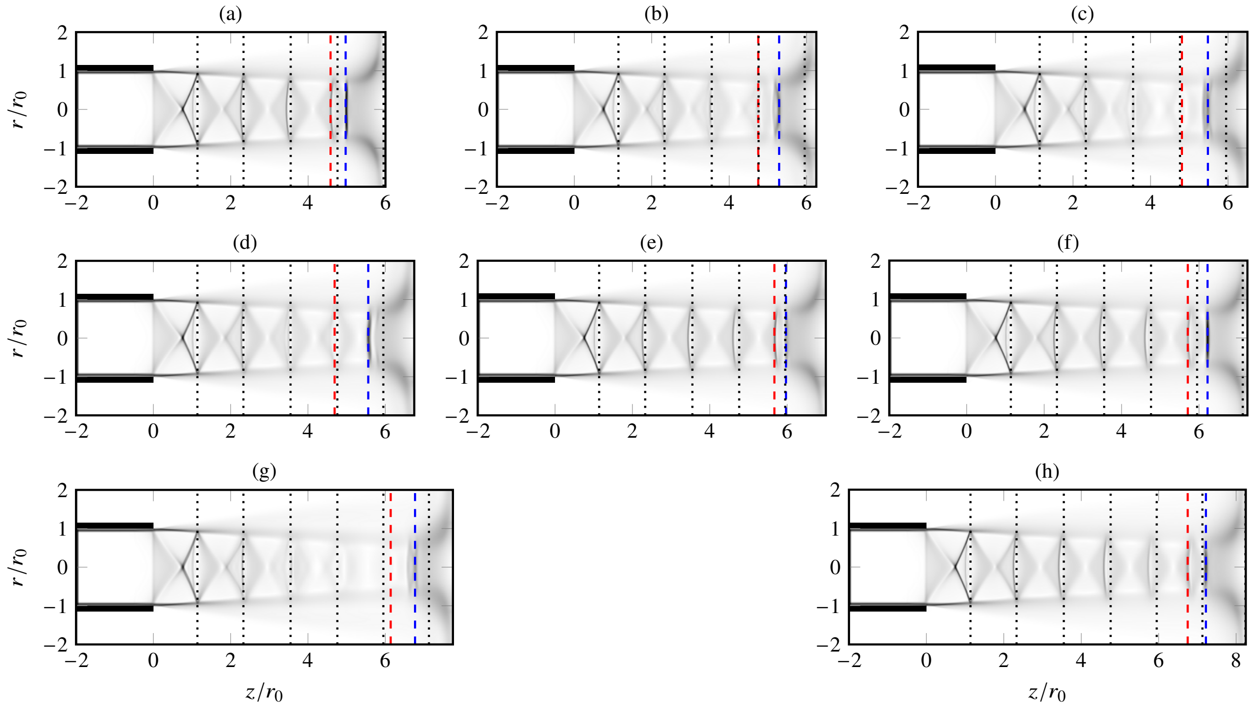

Fig. 10 Mean pseudo-schlieren fields in the (r, z) plane for $\mathrm{M}_j = 1.13$ for (a) $L = 6r_0$, (b) $L = 6.25r_0$, (c) $L = 6.5r_0$, (d) $L = 6.75r_0$, (e) $L = 7r_0$, (f) $L = 7.25r_0$, (g) $L = 7.75r_0$ and (h) $L = 8.25r_0$; mean axial positions of ········ the shocks for the corresponding free jet and of - - - - the last and - - - - the stand-off shocks in the impinging jets.

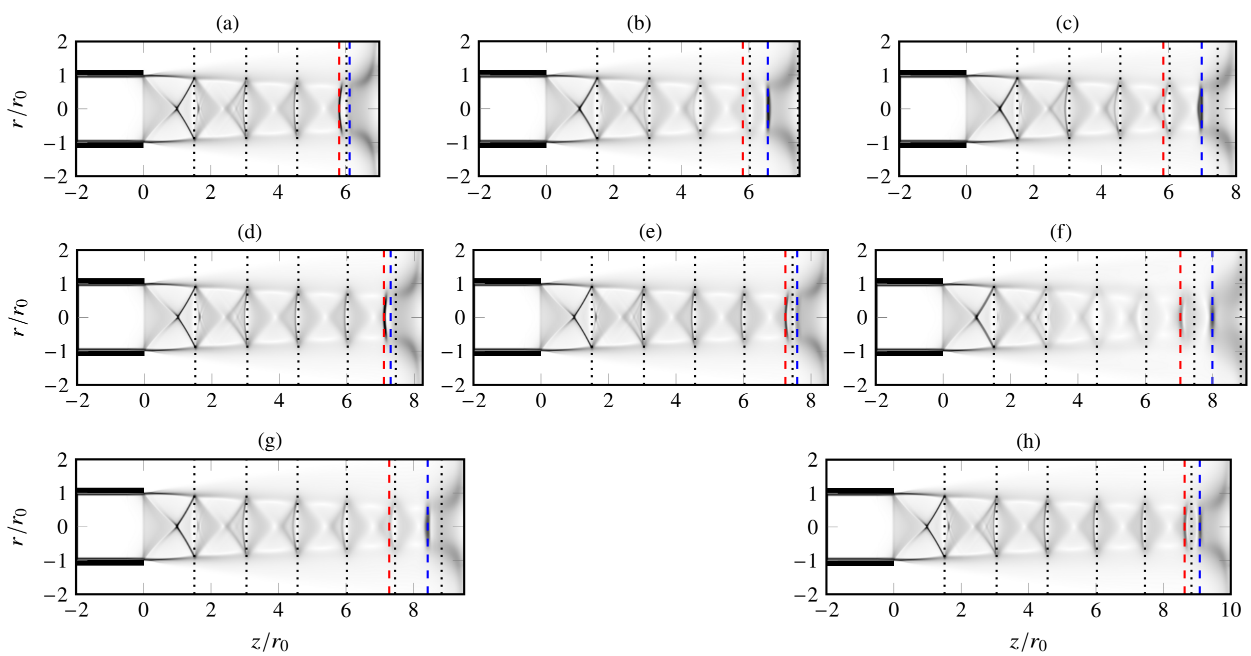

Fig. 11 Mean pseudo-schlieren fields in the (r, z) plane for $\mathrm{M}_j = 1.20$ for (a) $L = 7r_0$, (b) $L = 7.5r_0$, (c) $L = 8r_0$, (d) $L = 8.25r_0$, (e) $L = 8.5r_0$, (f) $L = 9r_0$, (g) $L = 9.5r_0$ and (h) $L = 10r_0$; mean axial positions of ········ the shocks for the corresponding free jet and of - - - - the last and - - - - the stand-off shocks in the impinging jets.

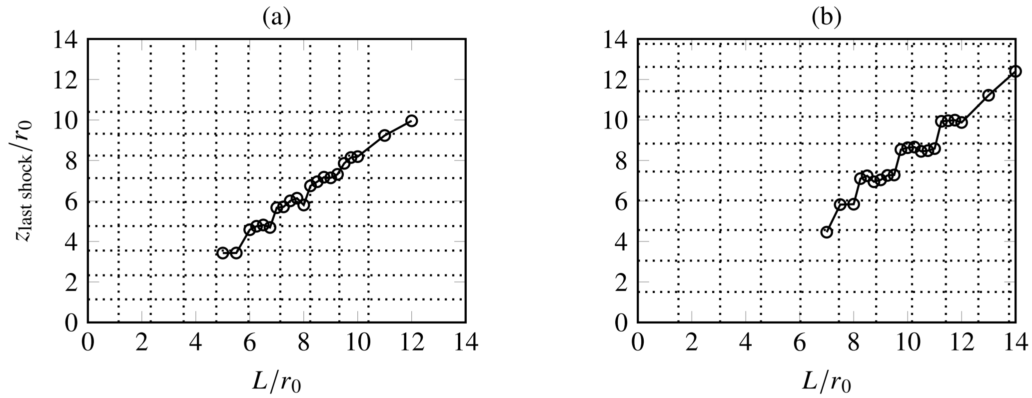

Fig. 12 Mean axial positions of the last shock in the shock-cell network for (a) $M_j = 1.13$ and (b) $M_j = 1.20$ as a function of the nozzle-to-plate distance ; ········ mean axial positions of the shocks in the free jets.

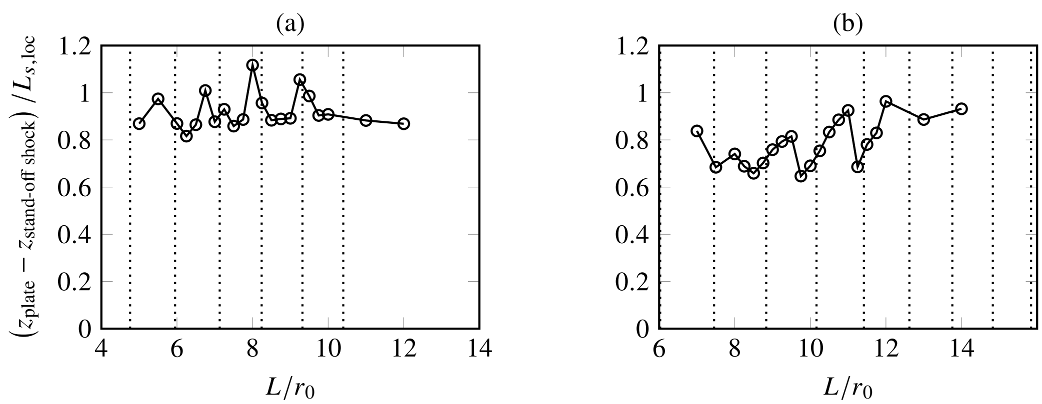

Fig. 13 Distance between the stand-off shock and the plate for (a) $M_j = 1.13$ and (b) $M_j = 1.20$ as a function of the nozzle-to-plate distance ; ········ mean axial positions of the shocks for the free jets.

jets at $M_j = 1.13$ and 1.20 are represented as a function of the nozzle-to-plate distance in figure 14. They are also normalized by the length of the local free-jet shock cell near the plate. The positions of the free-jet shocks are also indicated. For the two Mach numbers, the distances between the last shock and the stand-off shock range between 0.1 and 1. This range is wider than the one for the distance between the stand-off shock and the plate, in figure 13. For $6r_0 \lesssim L \lesssim 10r_0$ at $M_j = 1.13$ and for $8r_0 \lesssim L \lesssim 12r_0$ at $M_j = 1.20$, the distances between the last shock and the stand-off shock vary in a saw-tooth manner, increasing smoothly with the nozzle-to-plate distance when the plate is located between two shocks but decreasing sharply when it crosses a shock in the free jet.

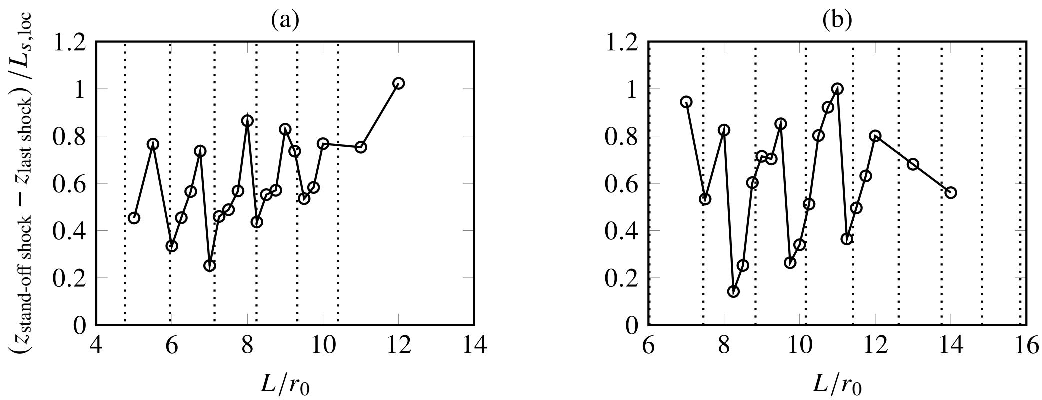

Fig. 14 Distance between the last shock in the shock-cell network and the stand-off shock for (a) $M_j = 1.13$ and (b) $M_j = 1.20$ as a function of nozzle-to-plate distance ; ········ mean axial positions of the shocks for the free jets.

Finally, to track the links between the shock positions and the tone amplitude, the amplitudes of the dominant tones for the impinging jets at $M_j = 1.13$ and 1.20 are represented in figure 15 as a function of the distance between the last shock of the shock-cell network and the stand-off shock, normalized by the free-jet shock cell length around the plate. For each jet, the value of the nozzle-to-plate distance is indicated above the marker. For the two Mach numbers, the amplitude of the dominant tone is overall higher when the distance between the last shock and the stand-off shock is larger. The amplitude is around 150 dB when the distance between the last shock and the stand-off shock is below $0.3L_{s,\text{loc}}$, but is around 170 dB when the distance is above $0.6L_{s,\text{loc}}$.

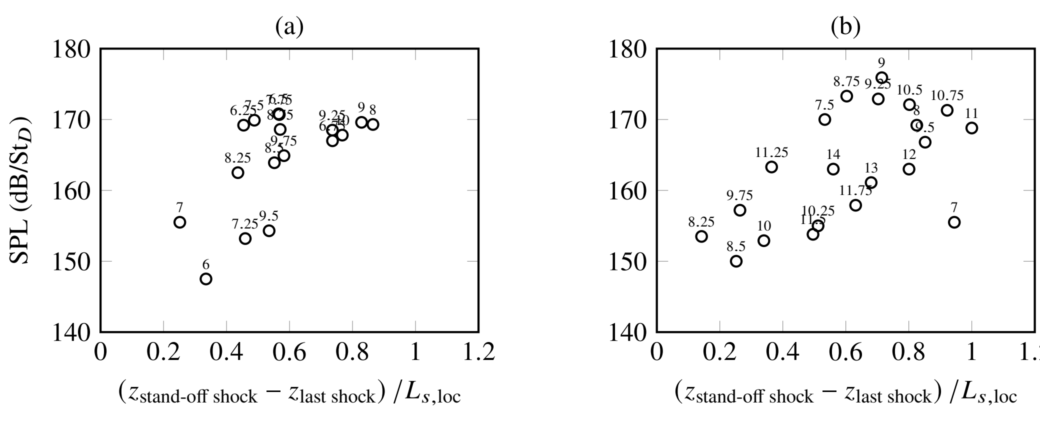

Fig. 15 Amplitudes of the dominant tones obtained at $r = 1.5r_0$ and $z = 0$ for (a) $M_j = 1.13$ and (b) $M_j = 1.20$ as a function of the distance between the stand-off shock and the last shock in the shock-cell network ; the nozzle-to-plate distance is specified above each marker.

IV. Conclusion

The tones produced by screeching jets impinging on a flat plate for Mach numbers $M_j = 1.13$ and 1.20 and nozzle-to-plate distances between $L = 5r_0$ and $16r_0$ have been investigated using large-eddy simulations. The screech tones are dominant and coexist with impingement tones for nozzle-to-plate distances higher than $L \gtrsim 10r_0$ and $12r_0$, for $M_j = 1.13$ and 1.20. For shorter distances, the impingement tones are stronger than the screech tones, whose amplitude becomes significantly weaker as plate is closer to the jet nozzle exit. When the stand-off shock is located close to the last shock of the shock-cell network, the impingement tones are weak. When this occurs, the plate is also located close to the position of a shock of the corresponding free jet. On the contrary, when the stand-off shock is far from the last shock in the impinging jet, the impingement tones are strong.

In this study, the amplitudes of the dominant impingement tones are linked to the distance between the stand-off shock and the last shock of the shock-cell network. This link suggests that the stand-off shock is involved in the near-plate mechanism producing the upstream-propagating components of the feedback loops establishing in impinging non-ideally expanded jets. This mechanism may be the interactions of the large-scale coherent structures convected in the mixing layers with the stand-off shock, producing noise similarly as for the screech resonance. The weakening of the impingement tones observed when the stand-off shock is very close to the last shock of the shock-cell network suggests that the noise-producing mechanism is less efficient in this case due to the proximity between the two shocks. Future work will be dedicated to identifying more precisely what causes the fluctuations in the amplitudes of the dominant impingement tones as the nozzle-to-plate distance varies. Such work could include a discussion on the near-plate noise generation mechanism of the feedback loop. Equivalent ideally-expanded impinging jets could also be simulated to investigate the effects of the presence or absence of a shock-cell network on the nozzle-to-plate resonance.

Acknowledgments

This work was granted access to the HPC resources of PMCS2I (Pôle de Modélisation et de Calcul en Sciences de l'Ingénieur de l'Information) of the École Centrale de Lyon, and IDRIS (Institut du Développement et des Resources en Informatique Scientifique) under the allocation A0172A00204 made by GENCI (Grand Équipement National de Calcul Intensif). It was performed within the framework of the LABEX CeLyA (ANR-10-LABX-0060) of Université de Lyon, within the program *Investissements d'Avenir* (ANR-16-IDEX-0005) operated by the French National Research Agency (ANR).

References

[1] Powell, A., ''The noise of choked jets,'' *J. Acoust. Soc. Am.*, Vol. 25, No. 3, 1953, pp. 385–389. https://doi.org/10.1121/1.1907052.

[2] Powell, A., ''On the mechanism of choked jet noise,'' *Proc. Phys. Soc. B*, Vol. 66, No. 12, 1953, pp. 1039–1057. https://doi.org/10.1088/0370-1301/66/12/306.

[3] Raman, G., ''Advances in understanding supersonic jet screech: review and perspective,'' *Prog. Aerosp. Sci.*, Vol. 34, No. 1, 1998, pp. 45–106. https://doi.org/10.1016/S0376-0421(98)00002-5.

[4] Raman, G., ''Supersonic jet screech: half-century from Powell to the present,'' *J. Sound Vib.*, Vol. 225, No. 3, 1999, pp. 543–571. https://doi.org/10.1006/jsvi.1999.2181.

[5] Edgington-Mitchell, D., ''Aeroacoustic resonance and self-excitation in screeching and impinging supersonic jets – A review,'' *Int. J. Aeroacoustics*, Vol. 18, No. 2, 2019, pp. 118–188. https://doi.org/10.1177/1475472X19834521.

[6] Norum, T. D., ''Screech suppression in supersonic jets,'' *AIAA J.*, Vol. 21, No. 2, 1983, pp. 235–240. https://doi.org/10.2514/3.8059.

[7] Umeda, Y., and Ishii, R., ''On the sound sources of screech tones radiated from choked circular jets,'' *J. Acoust. Soc. Am.*, Vol. 110, No. 4, 2001, pp. 1845–1858. https://doi.org/10.1121/1.1402620.

[8] Varé, M., and Bogey, C., ''Mach number dependence of tone generation by impinging round jets,'' *AIAA J.*, Vol. 61, No. 8, 2023, pp. 3551–3565. https://doi.org/10.2514/1.J062746.

[9] Bogey, C., and Gojon, R., ''Feedback loop and upwind-propagating waves in ideally expanded supersonic impinging round jets,'' *J. Fluid Mech.*, Vol. 823, 2017, pp. 562–591. https://doi.org/10.1017/jfm.2017.334.

[10] Nosseir, N. S., and Ho, C.-M., ''Dynamics of an impinging jet. Part 2. The noise generation,'' *J. Fluid Mech.*, Vol. 116, 1982, pp. 379–391. https://doi.org/10.1017/S0022112082000512.

[11] Ho, C.-M., and Nosseir, N. S., ‘‘Dynamics of an impinging jet. Part 1. The feedback phenomenon,’’ *J. Fluid Mech.*, Vol. 105, 1981, pp. 119–142. https://doi.org/10.1017/S0022112081003133.

[12] Edgington-Mitchell, D., Jaunet, V., Jordan, P., Towne, A., Soria, J., and Honnery, D., ‘‘Upstream-travelling acoustic jet modes as a closure mechanism for screech,’’ *J. Fluid Mech.*, Vol. 855, 2018, p. R1. https://doi.org/10.1017/jfm.2018.642.

[13] Gojon, R., Bogey, C., and Mihaescu, M., ‘‘Oscillation modes in screeching jets,’’ *AIAA J.*, Vol. 56, No. 7, 2018, pp. 2918–2924. https://doi.org/10.2514/1.J056936.

[14] Tam, C. K. W., and Ahuja, K. K., ‘‘Theoretical model of discrete tone generation by impinging jets,’’ *J. Fluid Mech.*, Vol. 214, 1990, pp. 67–87. https://doi.org/10.1017/S0022112090000052.

[15] Tam, C. K. W., and Hu, F. Q., ‘‘On the three families of instability waves of high-speed jets,’’ *J. Fluid Mech.*, Vol. 201, 1989, pp. 447–483. https://doi.org/10.1017/S002211208900100X.

[16] Edgington-Mitchell, D., Li, X., Liu, N., He, F., Wong, T. Y., Mackenzie, J., and Nogueira, P., ‘‘A unifying theory of jet screech,’’ *j. Fluid Mech.*, Vol. 945, 2022, p. A8. https://doi.org/10.1017/jfm.2022.549.

[17] Varé, M., and Bogey, C., ‘‘Generation of acoustic tones in round jets at a Mach number of 0.9 impinging on a plate with and without a hole,’’ *J. Fluid Mech.*, Vol. 936, 2022, p. A16. https://doi.org/10.1017/jfm.2022.47.

[18] Henderson, B., Bridges, J., and Wernet, M., ‘‘An experimental study of the oscillatory flow structure of tone-producing supersonic impinging jets,’’ *J. Fluid Mech.*, Vol. 542, 2005, pp. 115–137. https://doi.org/10.1017/S0022112005006385.

[19] Weightman, J. L., Amili, O., Honnery, D., Soria, J., and Edgington-Mitchell, D., ‘‘An explanation for the phase lag in supersonic jet impingement,’’ *J. Fluid Mech.*, Vol. 815, 2017, p. R1. https://doi.org/10.1017/jfm.2017.37.

[20] Varé, M., and Bogey, C., ‘‘Presence and properties of acoustic peaks near the nozzle of impinging rocket jets,’’ *Acta Acust.*, Vol. 6, 2022, p. 36. https://doi.org/10.1051/aacus/2022033.

[21] Edgington-Mitchell, D. M., Weightman, J. L., Mazharmanesh, S., and Nogueira, P., ‘‘Vortices, shocks and non-linear acoustic waves: the ingredients for resonance in impinging compressible jets,’’ *J. Fluid Mech.*, Vol. 1015, 2025, p. A56. https://doi.org/10.1017/jfm.2025.10383.

[22] Jaunet, V., Mancinelli, M., Jordan, P., Towne, A., Edgington-Mitchell, D. M., Lehnasch, G., and Girard, S., ‘‘Dynamics of round jet impingement,’’ *AIAA Paper 2019-2769*, 2019. https://doi.org/10.2514/6.2019-2769.

[23] Krothapalli, A., ‘‘Discrete tones generated by an impinging underexpanded rectangular jet,’’ *AIAA J.*, Vol. 23, No. 12, 1985, pp. 1910–1915. https://doi.org/10.2514/3.9195.

[24] Li, X., He, F., Zhang, X., Hao, P., Wu, X., and Liu, N., ‘‘Experimental study on acoustic resonance of subsonic and slightly underexpanded impinging jets,’’ *J. Fluid Mech.*, Vol. 983, 2024, p. A32. https://doi.org/10.1017/jfm.2024.27.

[25] Mancinelli, M., Meloni, S., and Camussi, R., ‘‘An experimental investigation of the resonance appearance in an impinging jet,’’ *AIAA Paper 2024-3374*, 2024. https://doi.org/10.2514/6.2024-3374.

[26] Tam, C. K. W., and Norum, T. D., ‘‘Impingement tones of large aspect ratio supersonic rectangular jets,’’ *AIAA J.*, Vol. 30, No. 2, 1992, pp. 304–311. https://doi.org/10.2514/3.10919.

[27] Norum, T. D., ‘‘Supersonic rectangular jet impingement noise experiments,’’ *AIAA J.*, Vol. 29, No. 7, 1991, pp. 1051–1057. https://doi.org/10.2514/3.10703.

[28] Krothapalli, A., Rajkuperan, E., Alvi, F., and Lourenco, L., ‘‘Flow field and noise characteristics of a supersonic impinging jet,’’ *J. Fluid Mech.*, Vol. 392, 1999, pp. 155–181. https://doi.org/10.1017/S0022112099005406.

[29] Dauptain, A., Gicquel, L. Y. M., and Moreau, S., ‘‘Large eddy simulation of supersonic impinging jets,’’ *AIAA J.*, Vol. 50, No. 7, 2012, pp. 1560–1574. https://doi.org/10.2514/1.J051470.

[30] Gojon, R., and Bogey, C., ‘‘Flow structure oscillations and tone production in underexpanded impinging round jets,’’ *AIAA J.*, Vol. 55, No. 6, 2017, pp. 1792–1805. https://doi.org/10.2514/1.J055618.

[31] Jia, Z., and Gao, J., ‘‘A numerical study on the zone of silence of the impinging tone from supersonic perpendicular impinging jets,’’ *Phys. Fluids*, Vol. 37, No. 8, 2025, p. 086173. https://doi.org/10.1063/5.0282903.

[32] Bogey, C., Marsden, O., and Bailly, C., ''Large-eddy simulation of the flow and acoustic fields of a Reynolds number 10^5 subsonic jet with tripped exit boundary layers,'' *Phys. Fluids*, Vol. 23, No. 3, 2011, pp. 035–104. https://doi.org/10.1063/1.3555634.

[33] Bogey, C., and Bailly, C., ''A family of low dispersive and low dissipative explicit schemes for flow and noise computations,'' *J. Comput. Phys.*, Vol. 194, No. 1, 2004, pp. 194–214. https://doi.org/10.1016/j.jcp.2003.09.003.

[34] Fauconnier, D., Bogey, C., and Dick, E., ''On the performance of relaxation filtering for large-eddy simulation,'' *J. Turbul.*, Vol. 14, No. 1, 2013, pp. 22–49. https://doi.org/10.1080/14685248.2012.740567.

[35] Berland, J., Bogey, C., Marsden, O., and Bailly, C., ''High-order, low dispersive and low dissipative explicit schemes for multiple-scale and boundary problems,'' *J. Comput. Phys.*, Vol. 224, No. 2, 2007, pp. 637–662. https://doi.org/10.1016/j.jcp.2006.10.017.

[36] Bogey, C., de Cacqueray, N., and Bailly, C., ''A shock-capturing methodology based on adaptative spatial filtering for high-order non-linear computations,'' *J. Comput. Phys.*, Vol. 228, No. 5, 2009, pp. 1447–1465. https://doi.org/10.1016/j.jcp.2008.10.042.

[37] Mohseni, K., and Colonius, T., ''Numerical treatment of polar coordinate singularities,'' *J. Comput. Phys.*, Vol. 157, No. 2, 2000, pp. 787–795. https://doi.org/10.1006/jcph.1999.6382.

[38] Bogey, C., de Cacqueray, N., and Bailly, C., ''Finite differences for coarse azimuthal discretization and for reduction of effective resolution near origin of cylindrical flow equations,'' *J. Comput. Phys.*, Vol. 230, No. 4, 2011, pp. 1134–1146. https://doi.org/10.1016/j.jcp.2010.10.031.

[39] Tam, C. K., and Dong, Z., ''Radiation and outflow boundary conditions for direct computation of acoustic and flow disturbances in a nonuniform mean flow,'' *J. Comput. Acoust.*, Vol. 04, No. 2, 1996, pp. 175–201. https://doi.org/10.1142/S0218396X96000040.

[40] Bogey, C., ''Grid sensitivity of flow field and noise of high-Reynolds-number jets computed by large-eddy simulation,'' *Int. J. Aeroacoustics*, Vol. 17, No. 4, 2018, pp. 399–424. https://doi.org/10.1177/1475472X18778287.

[41] Bogey, C., ''Acoustic tones in the near-nozzle region of jets: characteristics and variations between Mach numbers 0.5 and 2,'' *J. Fluid Mech.*, Vol. 921, 2021, p. A3. https://doi.org/10.1017/jfm.2021.426.

[42] Harper-Bourne, M., and Fisher, M. J., ''The noise from shock waves in supersonic jets - Noise mechanism,'' *AGARD-CP-131*, Vol. 11, 1974, pp. 1–13.